PAPER

The Use of Numerical Modeling to Optimize a New Wave Energy Converter Technology

AUTHORS

Brandon E. Green
Daniel G. MacDonald
School for Marine Science and Technology, University of Massachusetts Dartmouth

ABSTRACT

A numerical model of a new point-absorber wave energy converter (WEC) technology was designed for simulation purposes using Python. The governing equations were defined to take into account the relevant forces on the buoy in an ideal wave environment as well as any opposing forces due to damping, the power take-off (PTO) mechanism, and alternator. These equations of motion were solved using a high-order iterative process to study the linear kinematics of the buoy, the behavior of the PTO, and the associated power output in an ideal ocean wave environment. The model allows for the adjustment of relevant parameters to explore the behavior of the WEC and optimize system efficiency depending on the wave conditions. The numerical model was designed to run single simulations for a specified time interval; however, an optimization routine was implemented to optimize the mechanical parameters that greatly affect power output. The optimization portion of the model was implemented to study the response of the virtual WEC to a variety of input conditions pertaining to the buoy, PTO, and wave dynamics. This paper explains the development of the prototype WEC and the associated numerical model, in addition to evaluating the response of the WEC to a variety of input conditions. The output of the numerical model is discussed for the associated wave field used for simulation purposes. The design and implementation of the numerical model provides insight into changes in design components to maximize system power output and efficiency. The results of the numerical model and examples of data output for specific input conditions are investigated.

Keywords: ocean wave energy, numerical modeling, optimization

Introduction

Energy consumption is a challenging problem in today's world. The finite availability of fossil fuels is becoming a growing concern, in addition to potential contributions to the greenhouse effect. For these reasons, alternative energy research is gaining attention; however, there are major cost issues associated with renewables as compared to fossil fuel energy production (Callaghan & Boud, 2006).

The quest towards a future that has very little dependence on non-polluting energy sources is both long and arduous. Approximately 80% of the energy used today is from fossil fuels, and the World Energy Council anticipates a projected energy increase of 1.6% per year up to 2030 (Cruz, 2008). One of the largest energy debates worldwide is whether or not oil production has peaked as the global energy demand continues to increase (Sorensen, 2004).

Over the past several decades, renewable energy research in the United States has primarily focused on technology associated with the harvesting of solar, wind, biomass, and geothermal energies (Thorpe, 1998, 1999). There is no doubt that the research done in these fields is efficient and promising, but the best and most successful energy policy must take into account a wide range of renewable energy sources (Drew et al., 2009). Increasing the range of energy sources that can be harvested will ultimately provide more renewable sources to reduce base load operations from fossil fuel-based power plants. For this reason, ocean wave energy is gaining increased attention from governments, corporations, engineers, and scientists due to the significant amount of energy available in ocean waves (Falnes, 2007). It is estimated that 2 TW of energy, the equivalent of twice the world's electricity production, could be harvested from the world's oceans (Cruz, 2008). Many researchers and engineers are continuing to develop new and exciting technology to harvest the energy stored in the ocean (Pelc & Fujita, 2002). In order for wave energy to become an economically viable energy source, technology advancements capable of reducing capital costs and payback period for these devices must be achieved (Clement et al., 2002).

A significant body of research has been performed on wave energy conversion technologies over the last several decades. Here, we focus on select, recent projects relevant to point absorber technologies and our device design. Engstrom (2011) describes recent

and ongoing efforts to develop a system of point-absorber wave energy converters (WECs), recently tested off the west coast of Sweden, capable of producing a nominal power output of 10 kW. The point absorber systems evaluated were designed as a two-body system consisting of a cylindrical surface buoy coupled to a submerged body. The submerged body was then connected to a linear generator, which was moored to the ocean bottom. Engstrom (2011) also describes a detailed numerical model to simulate the response of these WECs in ocean conditions, which is in good agreement with their ocean test results. Agamloh et al. (2007) describe a new point-absorber technology utilizing a contactless force transmission system incorporating a magnetic coupling system similar in some respects to the coupling system designed for the WEC in this manuscript, as described in the World Intellectual Property Organization's (WIPO) Patent Cooperation Treaty (PCT) application PCT/US13/42597 (to be published on December 2013). The design of Agamloh et al. (2007) utilized a rotary direct-drive system that was constructed specifically to operate with a buoy directly coupled to a ball screw used as the power take-off (PTO) mechanism, which was allowed to spin only in one direction (during the upstroke of the buoy). During prototype testing, their WEC device was capable of producing close to 70 W of maximum power output (Agamloh et al., 2008). Ocean Power Technologies (OPT, 2010) has developed a deep-ocean point absorbing technology known as the PowerBuoy, which has been deployed in many testing locations since 2000. Various configurations of the OPT technology have utilized linear generators, hydraulic fluid, and most recently, a rack-and-pinion design.

Although there are many emerging technologies that are designed for ocean wave energy generation, the field is still in its infant stages. There are many challenges associated with designing for the ocean environment. Among these difficulties, designing for brutal marine environmental conditions, which include extreme forces, corrosion, and biofouling, is of primary concern. Longevity of these devices is an important feature, and yet, it is also desirable to design them for operation with minimal maintenance. One drawback to utility-scale generation is that the research and development timetable is long, and it may be a decade or more before viable offshore WECs will be routinely producing power for the electrical grid (Henderson, 2006). Our device proposes a new approach focused on the nearshore environment, where the research and development timetable can be realistically reduced to years instead of decades. The technology discussed here is designed to take advantage of structures close to shore, such as docks, marinas, and piers, to generate smaller amounts of electricity, on the range of 1 kW. Our device is also scalable, in that, once nearshore deployments are successful, utility-scale projects can be achievable with further development to meet the needs of the demanding offshore environment.

The Nearshore Wave Energy Project

The nearshore point absorber (NSPA) WEC technology was developed in part by a team of undergraduate mechanical and electrical engineers as part of their capstone senior design project. The project goal was to design a working prototype, which generates electricity from ocean waves. This prototype was part of a larger vision, in which wave attenuation systems could utilize wave energy technology to generate electricity in addition to dissipating and/or reflecting the wave energy. These students were responsible for building the initial first-generation prototype. Dry testing of the device in the laboratory demonstrated the capability of our prototype to generate electricity with a maximum power generation on the order of 100 W. The first-generation prototype has provided a proof of concept for a linear to rotary motion electricity generation method. There are many design challenges that were taken into account. These included a rugged mounting system, a water-tight protective housing for the PTO mechanism, and environmentally benign components.

Device Description

The device utilizes a cylindrical buoy as the primary means of capturing the heaving motion of the waves. The PTO converts the linear motion of the buoy into rotational motion. A high-efficiency ball screw is used as the PTO mechanism because it is capable of producing high torque output with minimal friction losses, which can then be harvested with an alternator. The alternator used in the first-generation prototype is a WindBLU Power three-phase permanent magnet alternator (PMA), which converts the rotational motion of the ball screw into electricity. This alternator, based on its performance specifications, yields relatively high power output (100–200 W) at an RPM range of 400–600. Protecting the vital mechanical/electrical components of the PTO mechanism from the brutal marine environment is a priority of the device design. Since the buoy is connected to the PTO with a series of magnets, the PTO mechanism is capable of operating safely in a tightly

sealed PVC tube isolated from the ocean environment.

Our goal for the nearshore market is to develop a basic WEC on the order of $1,000, with a mean output of up to 1 kW of power. These devices will take advantage of fixed infrastructure (piers, docks, breakwaters, etc. in the nearshore zone, or fixed/floating oil or wind platforms offshore) to reduce costs by eliminating the need for separate moorings or support infrastructure. The first prototype is intended as a proof of concept and contains many components that can be optimized and will be considered in the numerical model discussed later. The fully assembled design of the first-generation prototype can be seen in Figure 1.

Through dry testing of the device and the use of power monitoring equipment and software, we were able to obtain a maximum power output of 150 W in the laboratory through manual lifting of the buoy. There are many components of the NSPA WEC design that make it an ideal system for nearshore applications, and these components are subject to further investigation through testing and numerical simulation. The remainder of this manuscript will show the mathematical model used in the simulation, explore the numerical model, discuss results and optimization, and report conclusions.

FIGURE 1

(a) SolidWorks drawing and first conceptualization of the NSPA WEC. (b) The first-generation prototype of the NSPA WEC.

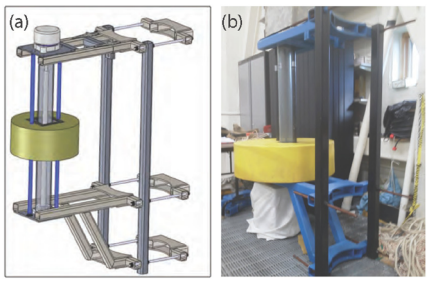

Mathematical Formulation and Relevant Equations

Numerical models are a valuable tool for understanding how the ocean environment will impact the mechanical and electrical components of a WEC (Ivanova et al., 2005). Access to this kind of information is extremely important in order to design for specific environmental conditions. The purpose of this section is to introduce the mathematical framework used to describe wave motion and account for any physics, which will affect the WEC in a wave environment. Simplified linear wave equations that represent the input of ocean waves are used for the numerical model. The expression for surface wave elevation, η_ω for a particular wave frequency, can be expressed as follows:

$$\eta_\omega(x,t) = \frac{H}{2}\sin(kx - \omega t), \qquad (1)$$

where H is the wave height, k is the wave number, and ω is the angular wave frequency. This expression for the surface height of the ocean waves is important because it creates the buoyancy force used to drive the system. The energy associated with the heaving motion of the buoy is the energy of interest for extraction.

The dispersion relationship is a basic equation that relates the wave speed, wavelength, and water depth. This equation also is an expression for the relationship between frequency and wave number as well as between period and wavelength. This equation can be useful for determining the wavelength when the water depth and wave period are known. The dispersion relation can be written as follows (Kundu & Cohen, 2008):

$$\omega^2 = kgtanh(kh), \qquad (2)$$

where g is the gravitational constant, h is the water depth, and ω is the wave frequency.

Relevant equations that represent the dynamics of the NSPA WEC system are also developed, which include buoy, ball screw, and alternator specifications. The goal of this manuscript is to outline the modeling approach used for the NSPA WEC device, which will be used to define the optimal mechanical configuration of the device.

NSPA WEC Theory

To properly build a mathematical model of the NSPA WEC, all relevant forces must be considered that pertain to the operating wave environment and the physics of the WEC system. The important dynamics of the WEC system, which will be introduced in this section, consist of three components that affect how the machine will operate. These components are the buoy, the PTO, and the three-phase alternator. The system operates as follows: the heaving motion of the buoy, which is magnetically coupled to a ball nut, transfers energy into the PTO, which is then translated into rotational motion. This rotational motion is then used to drive the primary rotor inside the alternator, which produces electric power output.

Mechanical Components

To model the NSPA, it is important to take into account the forces active on the system and any damping effects. The forces acting on the buoy can be seen in Figure 2. These forces

FIGURE 2

Diagram of the forces on the NSPA WEC during operation in a wave environment.

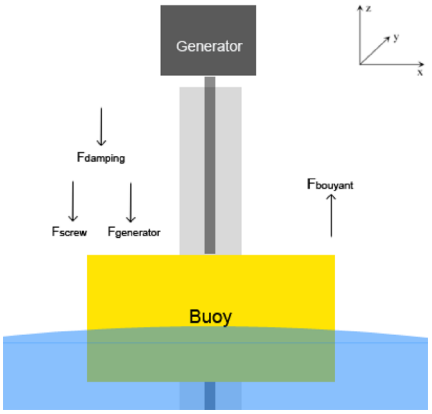

account for any damping effects related to the ball screw and alternator, the buoyancy force, and the inertial forces from the screw and alternator.

First, consider the buoyant force acting on the buoy when an idealized wave passes. This force is important because it is the driving force of the system. The buoyant force is defined as follows:

$$F_{bouyancy} = \Delta\rho A_b g \Delta z \tag{3}$$

where $\Delta\rho$ is the difference between the density of the fluid and the density of the float, A_b is the cross-sectional area of the buoy in the x–y plane, and Δz is the amount of the buoy that is submerged. Δz is expressed as $\eta(x, t) - z(t)$, where $\eta(x, t)$ is the surface wave height, and z is the buoy position. As the surface height of the waves changes, the submerged buoy volume changes, which drives the system.

Next, consider forces pertaining to the ball screw. Since the ball screw is converting linear motion into rotary motion, the screw will have a moment of inertia, a constant brake that opposes the motion, and torque losses associated with it. We can express the forces on the ball screw as follows:

$$F_{screw} = \frac{2\pi}{l}(K_s\omega + To_s + I_s\alpha). \tag{4}$$

where l is the lead of the ball screw in m/rad, K_s is the breaking coefficient associated with the ball screw, To_s is the torque losses from the screw, I_s is the moment of inertia of the screw, and w and α are the angular velocity and acceleration, respectively.

The third component of the equation of motion is related to the inertial generator forces. Since the ball screw is directly coupled to the generator, the rotational motion of the screw is used to drive the alternator. Because the alternator is also spinning, there will be a moment of inertia and a back torque, which opposes the forward driving of the system. The forces from the generator can be expressed as follows:

$$F_{generator} = \frac{2\pi}{l}(K_g\omega + To_g + I_g\alpha). \tag{5}$$

where K_g is the breaking coefficient associated with the generator, To_g is the torque losses from the generator, and I_g is the moment of inertia of the generator.

The last of the forces, which is important to consider, are the damping forces. The damping forces scale with linear velocity terms, and the main coefficients to consider are associated with hydrodynamic and generator effects. The damping force is as follows:

$$F_{damping} = C\dot{z}, \tag{6}$$

where $C = C_{hd} + C_{gen}$ is the damping coefficient associated with this system and is made up of hydrodynamic and generator components. The hydrodynamic damping portion of the damping term is concerned with how much of the buoy is submerged and can be shown as follows:

$$C_{hd} = \frac{\pi^2\rho g^2\bar{A}^2 D}{8\omega_n^3}, \tag{7}$$

where A is the ratio between the wave position and the buoy's position, D is the buoy diameter, and ω_n is the natural frequency of the buoy in heave (McCormick, 2010). The natural frequency of the buoy is defined as $\omega_n = \sqrt{\rho A_b g/m}$, where m is the buoy mass and A_b is the cross-sectional area of the buoy in the x–y plane.

The generator damping term is associated with the resistance in the circuit, the velocity of the buoy, and how much power is generated. This damping term changes as the speed of the buoy increases, and the stator coils inside the alternator become fully excited. This effectively limits the speed of the buoy as the power reaches the maximum load. The coefficient can be expressed as follows (Eriksson, 2007):

$$C_{gcn} = \frac{1}{R}\left(\frac{V}{\dot{z}}\right)^2$$

where R is the load resistance, V is the voltage produced, and $\dot{z}$ is the velocity of the buoy.

When looking at this system, the effects from the screw, generator, and damping terms all oppose the driving buoyancy force acting on the buoy. Because the ball screw is highly efficient, the breaking coefficient K_s and, therefore, the loss torque To_s associated with the screw are negligible, as compared to the breaking coefficient and loss torque associated with the alternator. The force balance can now be expressed for the system as follows:

$$F_{bouyancy} - F_{damping} - F_{screw} - F_{generator} = m\ddot{z} \tag{8}$$

where m is the mass of the buoy and $\ddot{z}$ is the vertical acceleration of the buoy. Note that added mass associated with the buoy motion is not expected to be significant, as buoy accelerations are generally small, and at least when optimized, there is negligible relative motion between the buoy and the surrounding fluid. The numerical model utilizes linear wave theory, which requires inviscid fluid flow around the buoy. Added mass is directly related to the acceleration of the fluid due to viscous effects and is therefore of the second order and may be neglected. Substituting in for these terms, an equation of motion for the system is obtained, which can be solved through an iterative process, as follows:

$$\ddot{z} = \frac{1}{(1+A_5)} \cdot \{A_1(\eta - z) - (A_2 + A_3)\dot{z} - A_4\}. \quad (9)$$

where $A_1 = \frac{\rho A_g}{m}$, $A_2 = \frac{C}{m}$, $A_3 = \frac{(2\pi)^2 K_g}{l^2 m}$, $A_4 = \frac{2\pi}{lm}\, To_g$, and $A_5 = \frac{(2\pi)^2 I}{l^2 m}$.

Equation 9 is the defined differential equation and equation of motion that can be used to step through time, given the initial buoy position and velocity using a high-resolution iterative process. Once the linear kinematic information is obtained, dynamics of the specific components in the system such as the ball screw and alternator effects can be studied further. Rotational information can easily be collected, and the ball screw operating frequency can be used to calculate power output. The equations, which are important for obtaining power output, will be introduced in the next section.

Electrical Components

When considering an alternator, there are many important characteristics that must be taken into account. Some of these parameters are rotor dimension, magnetic field strength, number of stator coils, the amount of wire turns in these coils, and the air gap between the rotor and stator (Bostrom, 2011, 27-28).

The electromagnetic behavior of the generator can be studied using a field model. Electromagnetic field theory describes the complex phenomena related between electrical and magnetic effects. The fundamental laws of electromagnetism can be represented using Maxwell's equations, and the primary equation utilized is as follows (Griffiths, 1999):

$$\nabla \times \mathbf{E} = -\frac{\partial \mathbf{B}}{\partial t}, \quad (10)$$

where **E** is the electric field and **B** is the magnetic flux density. This equation is a mathematical description of Faraday's Law, which states that, when the magnetic flux changes, there is an electromotive force that induces a voltage in a closed circuit loop. This theory, when applied to alternators, brings rise to multiple instances of closed loop circuits consisting of N amount of turns to create stator coils. The rotor is the primary moving mechanism inside an alternator, which consists of strong magnetic field elements that spin to create a changing magnetic flux through the stator coils. The induced voltage, or electromotive force (EMF), which is related to how the magnetic flux changes through the coils, is expressed as follows (Griffiths, 1999):

$$EMF = -N \cdot \frac{d\Phi}{dt}, \quad (11)$$

where Φ is the magnetic flux and N is the number of wire loops in the stator coil. The primary mover, in this case, the ball screw, is the input mechanism that will be used to move the rotor and charge the stator coils to produce a voltage.

For a three-phase AC alternator, substituting for the magnetic flux Φ, the total RMS power can be obtained with the following expression (Simoes & Farret, 2004):

$$P_{rms} = \frac{(NBA\omega_r)^2}{2R\sqrt{2}}. \quad (12)$$

The relevant equations, which describe the NSPA WEC, have been presented and are utilized in the model simulations. In regards to these equations, the alternator model is intended to account for a resistive load only. This is to simplify the model and force the electrical system to enable the immediate reaching of the maximum current for a given electrical resistance. These equations can then be utilized with the intention of numerical model development for the dynamics of the WEC system. This numerical model will ultimately permit the study of the effects of the relevant buoy, PTO, and alternator parameters for system optimization.

The NSPA WEC Numerical Model

A fourth-order Runge–Kutta ordinary differential equation solver (Press, 2007) was utilized for the iterative process of stepping the equation of motion through time and solving for variables of interest. In addition to solving single cases of the WEC in operation, an optimization method was also developed. The optimization method was designed to aid in finding

the most efficient mechanical design configuration for specified wave input conditions.

Model Structure

Before presenting the full working numerical model, it is important to understand how the individual pieces are assembled for solving the equation of motion. The model has many components designed to handle separate tasks. The main component of the numerical model is the single case solver, which can be used to optimize the mechanical configuration of the device. The single case solver is designed to run one instance of the simulation and report on the performance of the WEC for the specified input conditions and system configuration. The single case solver is run for multiple simulations to output data, which can be analyzed to obtain the optimized configuration for the WEC in the model.

The single case solver reports on the performance for one specific simulation. The single case solver can be utilized for optimization purposes as well. Optimizing the components of the WEC requires running multiple instances of the single case solver for the variables the user is interested in to observe how the system performs for chosen specified design inputs. The optimization section of the code is designed to determine the average power output for the specified variables of interest. For example, the optimization method can be used to determine the range of values for the buoy radius and screw lead, which give the best power output for a given sea state.

The Single Case Solver

The input section of this code is designed to preset all of the conditions for the calculations portion, including buoy variables, initial position, time-related variables, ball screw specifications, and alternator parameters. The calculations section of the model is designed to take the input conditions and perform calculations to set up coefficients and other important variables crucial to the solver portion of the model, including functions related to the inertial components of the PTO and alternator, buoy dimensions, coefficients for the equation of motion, and velocity-independent damping coefficients related to the alternator. These variables are determined before the iterative processes associated with solving the equation of motion.

The wave field section of the model is designed to set up the wave conditions the user wishes to force on the virtual WEC. This portion of the model allows the user to designate the period, depth, and amplitude of the wave. The simulation then proceeds to calculate relevant variables such as the wave frequency and wave length. The model uses a secant solver method to solve the dispersion equation. The secant method of solving the two equations uses an iterative process to calculate the intersection between two functions.

The core of the model is the calculations performed at each time step during the iterative process. The relevant parameters, which are affected by time-varying properties, include the kinematics of the buoy and ball screw and power-related calculations.

Another important part of the calculations that happens with each iteration is the amount of damping present in the system. The linear damping term is a function of both the hydrodynamic and alternator damping terms. The hydrodynamic term depends on how much of the buoy is submerged into the water as the wave passes. The alternator damping term depends on the resistive load (set as a constant for our simulations), the velocity of the buoy, and the current power output at the associated time step. There are challenges related to keeping the damping term stable when the buoy velocity goes to zero. When the buoy is not moving, the damping term has a tendency to exhibit discontinuities over the run time. To avoid this numerical error, a threshold was implemented so that, when the velocity is less than 0.001 m/s, the generator damping coefficient is effectively zero.

The buoyancy force is calculated by dividing the buoy into individual horizontal length elements, dx, which are perpendicular to the passing wave crests, and by calculating the buoyancy force for every segment. These values are then summed up for the span of the buoy to determine the total buoyancy force. This is important, particularly for buoy radii on the order of the wavelength, where variations in buoyant forces across the buoy cannot be well represented by buoyant forces at the center of the buoy. The code accounts for 100 total buoyancy calculations, which include each individual buoy element along the horizontal.

The equation of motion is calculated using the previously determined coefficients and the initial conditions of the buoy. The calculation returns the next position of the buoy, which is then reiterated through the equation of motion. This process is performed for the designated run time defined in the input section of the model. The final set of calculations performed is related to the power output of the system. The power calculations implement the equations defined in the previous chapter, which define how an alternator delivers power as a function of mechanical input. The load circuit designed for this WEC system is a

constant resistive load. For each iteration, the RMS power is stored in an array for processing.

The last step before the data export is for all of the information to be processed and stored using the solver section of the code. The solver is designed to use all of the information calculated and utilize the equation of motion to produce all relevant data pertaining to the virtual WEC.

Numerical Model Simulations and Results

The optimization process runs multiple simulations for the variables of interest, records the RMS power for each configuration, and stores these values for plotting or data export. The process can be utilized multiple times to zone in on precise model parameters for a given wave field. In the examples discussed below, the wave period was held constant for the optimization process, which focused on changes to the buoy radius and ball screw lead. For these simulations, the alternator parameters are also held constant and designed to match the alternator used in the first-generation prototype. This section will report on the results for wave amplitudes of a = 0.125, 0.25, 0.50, and 0.75 m, respectively. These values were chosen to reflect wave amplitude values that are typically seen near the shore, as determined from wave data collected from the Clarks Cove test site located at the School for Marine Science in New Bedford, MA. The wave period associated with each amplitude was defined as T = 1 s, and the water depth was 10 m. The simulation responses for the wave period of T = 1 s were chosen because they showed the widest response range for the buoy radius and screw lead values at the specified wave amplitudes. The efficiency of the device was calculated using the ratio of the average power generated by the device to the wave energy flux per buoy diameter. The wave energy flux is calculated using the following equation (McCormick, 2010):

$$\bar{J} = c \cdot \bar{E}_{total} = \frac{1}{2}\rho g a^2 \left[\frac{1}{2}(1+G)\right] \cdot c, \tag{13}$$

where $G = \frac{2kh}{\sinh(2kh)}$, c is the wave speed, ρ is the density of seawater, and J is the wave energy flux per unit length of wave crest.

Optimizing Mechanical Components

Preliminary analysis with the single case solver indicated that buoy radius and screw lead were the parameters of highest priority for the optimization simulation. Thus, the objective was to determine optimal power output for a buoy radius range of 0.4–4.0 m and ball screw leads in the range of 0.01–0.1 m/rad. The optimization simulation was run for these buoy radii and screw leads for the specified wave amplitudes and a variety of wave periods, T. Here, we focus on the results for T = 1 s, which exhibited the widest dynamic range for the chosen wave amplitudes.

Figure 3 shows the effect of varying the buoy radius and the screw lead on power output and efficiency. The column on the left represents the average power output (W), while the column on the right represents the efficiency. Each row corresponds to the wave field, with the amplitude increasing down the rows. The color scale for the power output as well as the efficiency is equivalent for all of the plots in Figure 3. For all screw leads, the average power output does not reach high power outputs until the radius is large (>2.5 m). Since the buoyancy force scales with the buoy radius, it follows that the small leads (<0.03 m/rad) would not see considerable power output until the buoy radius was large enough for the buoyancy force to overcome resistive forces and drive the system. According to the data presented in Figure 3, the most efficient configuration for this wave field is for buoy radii near 3.5 m and for ball screw leads close to 0.03 m/rad. However, if the ball screw were to be constructed with lead values near 0.02 or 0.04 m/rad, there is a considerable decrease in power output for the specified wave field for buoy radii values close to 3.5 m.

The average power output is shown in the left column of Figure 3 for varying wave amplitudes at T = 1 s. For amplitudes a = 0.125 and 0.25 m, the power output is low (<2 kW) compared to the other higher wave amplitudes. The highest average power output values occur for all wave amplitude cases at ball screw leads close to 0.03 m/rad and a buoy radius near 3.5 m. By increasing the wave amplitude to a = 0.5 m, there will be a significant increase in the average power output of about 5 kW. This increase can be attributed to the high amount of buoyancy force at the optimal buoy radii and ball screw lead as well as a greater amount of instantaneous change in the buoyancy force compared to the wave amplitudes of less than a = 0.5 m. The higher amplitudes allow the system to overcome the resistive forces greater than the previous wave amplitudes. The final simulation for a = 0.75 m shows the maximum average power output increasing to 8 kW. The average power output plots reveal that, for increasing wave amplitudes, for buoy radii close to 3.5 m,

FIGURE 3

Optimization of buoy radius and screw lead for wave amplitudes of a = 0.125, 0.25, 0.5, and 0.75 m, respectively at wave period T = 1 s. Left column: buoy radius and screw lead with average power output (W). Right column: buoy radius and screw lead with efficiencies (%). (Color versions of figures are available online at http://www.ingentaconnect.com/content/mts/mtsj/2013/00000047/00000004.)

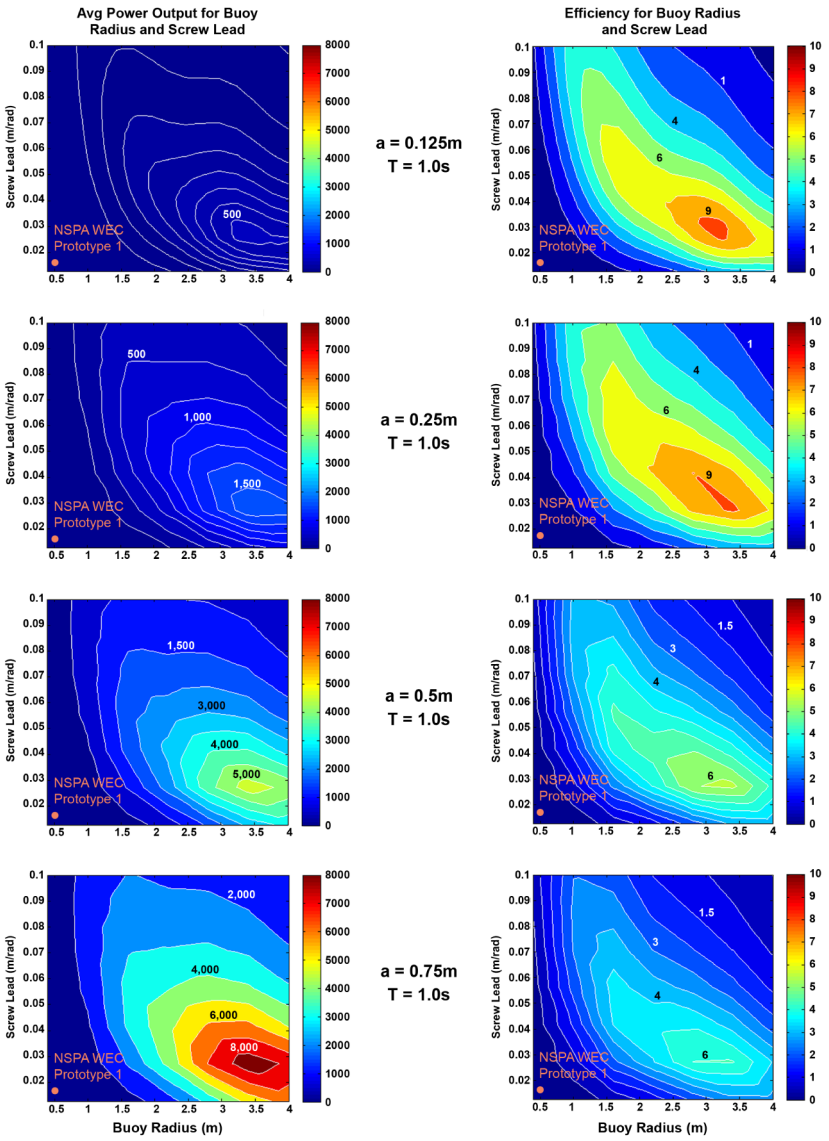

and for ball screw leads near 0.03 m/rad, the power output increases significantly between cases.

The efficiencies for each simulation are displayed in the right column of Figure 3 for the same varying wave amplitudes in the left column at T = 1 s. The efficiency associated with a = 0.125 m is near 9% for the first simulation. At a = 0.25 m, the efficiency remains the same (~9%) at buoy radii near 3.5 m, and ball screw leads close to 0.03 m/rad; however, the area surrounding this optimized range has decreased considerably from the case of a = 0.125 m. By increasing the wave amplitude to a = 0.5 m, the increase in buoyancy force yields a higher power output than the previous amplitudes; however, the maximum efficiency for the optimized buoy radii and ball screw leads decreased to 6%. Similarly, for the final wave amplitude of a = 0.75 m, there is an increase in the power output, and the efficiency remains at 6% for the optimized buoy radii and ball screw leads. Although the maximum efficiency remained the same, the area around the optimized buoy radii and ball screw lead values has decreased. The decrease in efficiency is attributed to the phase difference between the buoy and the wave for the cases of a > 0.25 m. The waves and the buoy are less in sync than the case of a = 0.125 and 0.25 m, allowing less opportunity for maximized power extraction. The effective area for the 6% efficiency of the optimized buoy radii and ball screw leads has decreased from the case of a = 0.50 m to the case of a = 0.75 m as well. This decrease in the effective area is due to the force balance between the gravitational and buoyancy forces. Finally, the figure shows that the efficiency of the NSPA WEC for these wave amplitudes at T = 1 s peaks at the inputs of a = 0.125 and 0.25 m and decreases for higher wave amplitudes.

The optimized values determined for the buoy radii and screw leads obtained through these simulations agree that the system configuration for the buoy radius and screw lead should be constructed for a buoy radius of 3.5 m and a ball screw lead of 0.03 m/rad for the given sea state. The extreme size of the optimized radius of the buoy is a significant design concern for a nearshore application. However, this value range for the buoy radius is not unexpected. As stated previously, the alternator used in the first-generation prototype and in this simulation is utilized for wind turbines. The required high

torque to utilize this alternator can be attributed to the length of wind turbine blades, which gives evidence to the model producing high buoy radius values for the optimal power output. The required high buoy radius, in addition to the poor efficiencies, shows that the alternator variables are severely limiting the system performance. These variables, in addition to those discussed in the Electrical Components section, include the torque required to turn the alternator and the load applied. These variables will be addressed in future designs by exploring different alternator configurations.

Optimized System Performance

After the optimization was performed for the wave conditions presented, the optimized values for the radius of the buoy and the ball screw lead were used to assess system performance in greater detail and investigate how the system behaves when the forces are balanced and efficiencies are maximized. For comparison purposes, the single case solver was run using the specifications of the first-generation prototype. This simulation response can be seen in Figure 4. Figure 4A is a position versus time plot showing the position of the buoy z_b, the water level z_w, and how much the buoy is submerged (dz). Figure 4B is a plot showing the buoy velocity and screw rotational speed, and Figure 4C is a plot showing the forces active during the simulation where F_b is the buoyancy force, F_{rot} are the screw/generator forces, and F_{net} is the total force. The last plot, Figure 4d, shows the power output, the output EMF, and the buoy's position relative to the EMF output. It is clear from Figure 4 that the system is operating poorly. The buoy has very little reaction to the wave field, due to the damping forces nearly canceling out the buoyancy

FIGURE 4

Simulation with NSPA WEC first-prototype specifications. Rbuoy = 0.5 m and lead = 0.0127 m/rad for T = 1 s and a = 0.25 m. (A) Buoy height (zb), wave height (zw), and their difference (dz). (B) buoy vertical velocity (w), vertical acceleration (az), angular velocity (o), and angular acceleration (ar). (C) Buoyant force (Fb), linear damping forces (Flin), and inertial forces (Frot). (D) EMF output and power output.

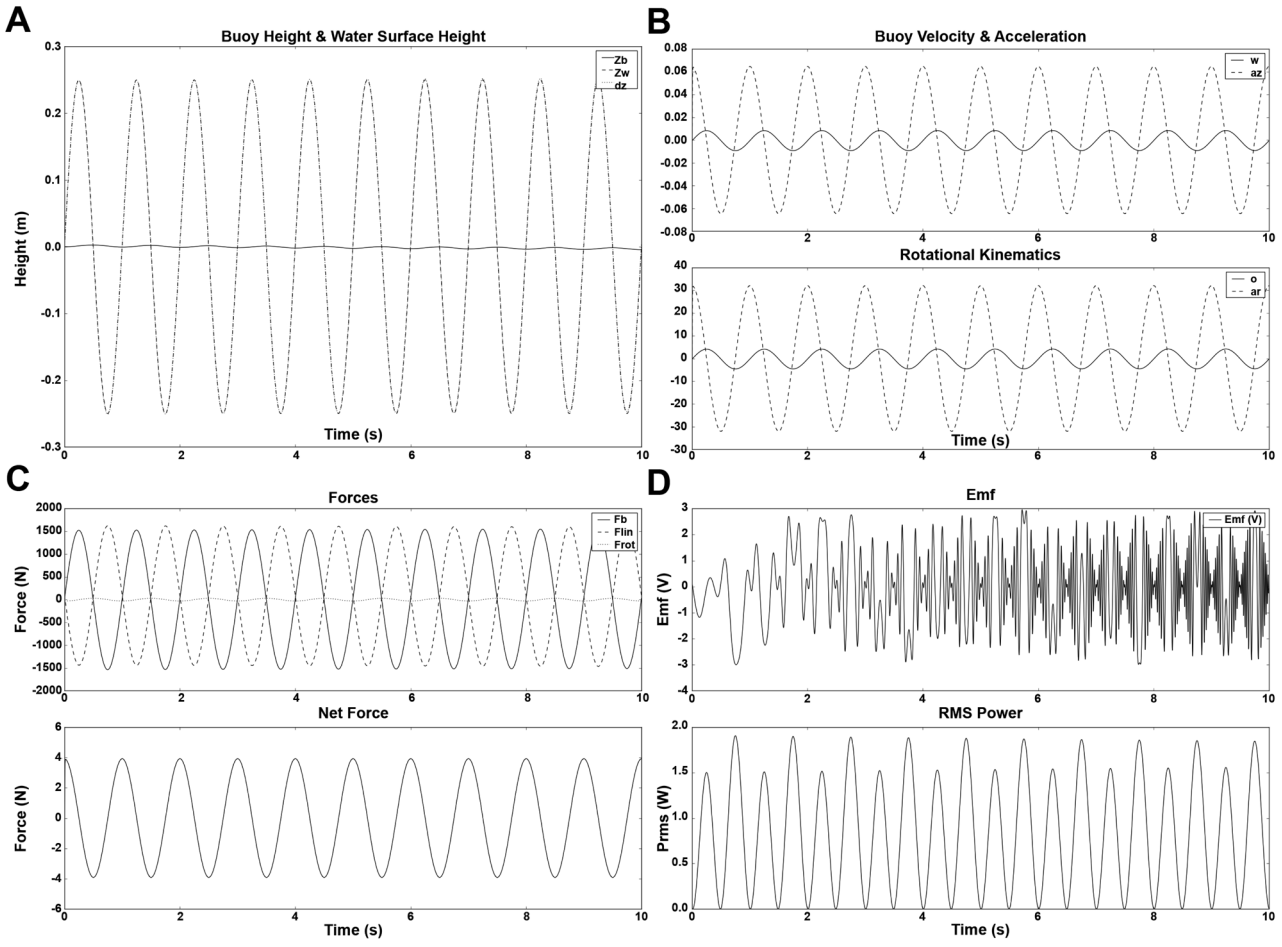

forces, as shown in Figure 4C. Since the rotational output is directly coupled to the movement of the buoy, the rotational speeds are low, yielding low power output. After the optimization determined the values of Rbuoy = 3.5 m and lead = 0.03 m/rad, the simulation was performed for the same sea state for comparison.

The results shown in Figure 5 are labeled the same as Figure 4 and are not plotted on the same scale due to their drastic difference in performance. Figure 5 reflects the simulations for the previously determined optimized values of Rbuoy = 3.5 m and lead = 0.03 m/rad for the a = 0.25 m and T = 1 s sea state. From the buoy position graph in Figure 5A, the buoy is able to track the wave more consistently than in Figure 4A. The buoy's amplitude of motion, z_b, and the water surface height, z_w, are now similar wave forms so that their difference (dz) is minimized. The full range of motion the buoy experienced permitted increased rotational speeds in the ball screw and higher power output, which can be seen in the RMS Power plot in Figure 5D. The net force is much higher in Figure 5C, which allows the system to drive and create higher power output than the results shown in Figure 4D. The power obtained through optimization increased to consistent 3500 W of peak RMS power after the transient effects died off near 1 s. The results of Figure 5 compared to Figure 4 show that the optimization routine was successful in obtaining the desired mechanical parameters for this system to use in the defined sea state.

Conclusion and Discussion

The ability to simulate WEC devices in an idealized ocean environment is a significant advantage for the

FIGURE 5

Simulation with determined optimized variables: Rbuoy = 3.5 m and lead = 0.03 m/rad for T = 1 s and a = 0.25 m. (A) Buoy height (zb), wave height (zw), and their difference (dz). (B) buoy vertical velocity (w), vertical acceleration (az), angular velocity (o), and angular acceleration (ar). (C) Buoyant force (Fb), linear damping forces (Flin), and inertial forces (Frot). (D) EMF output and power output.

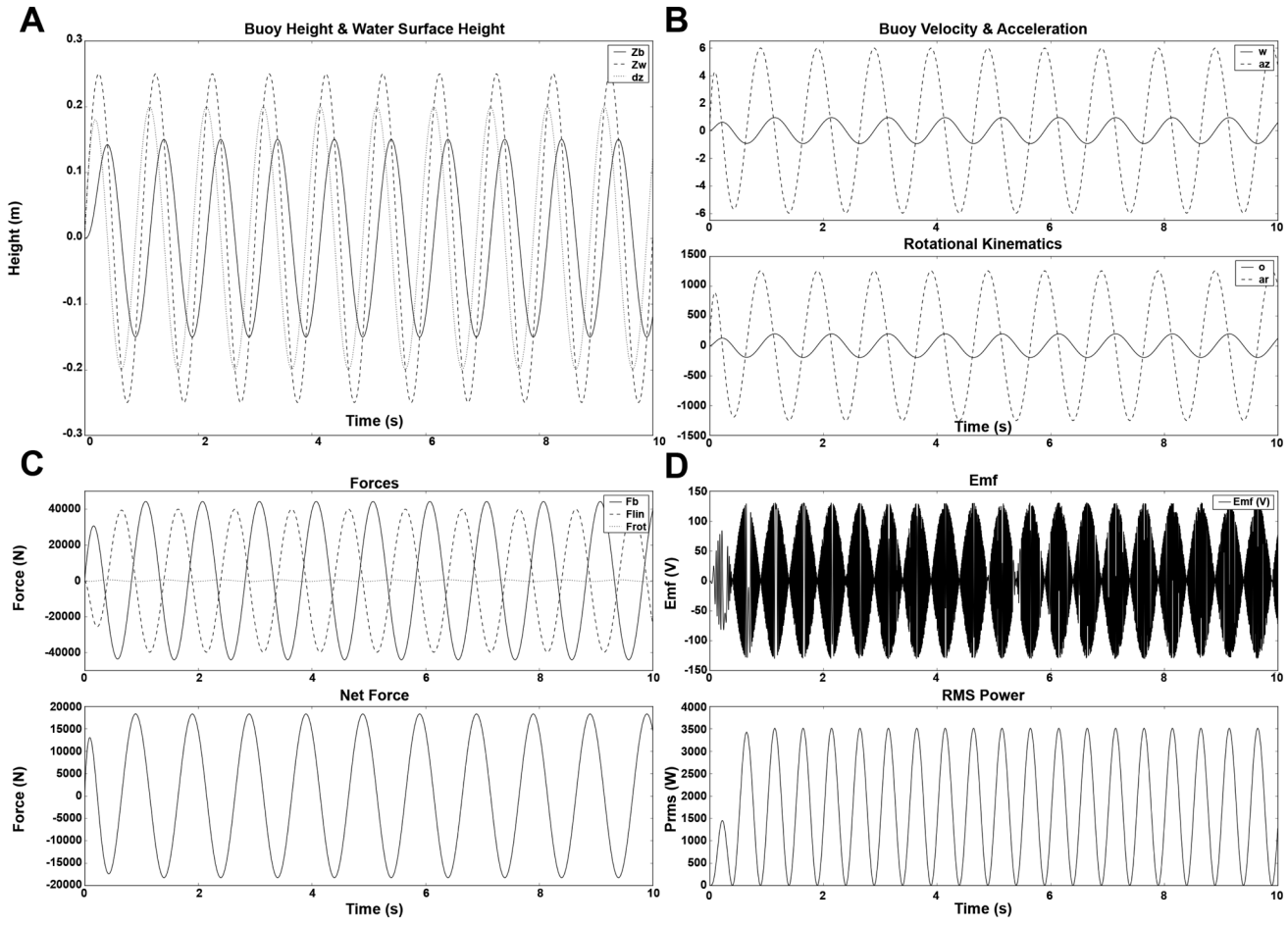

development of renewable energy devices for the ocean environment. Utilizing a detailed numerical model is extremely useful, allowing engineers and scientists to save on development cost by avoiding the construction of intermediate prototypes and decrease deployment time frames through the rigorous study of new designs before launch. The NSPA WEC prototype was utilized to study relevant physics related to the device and assist in the design of a numerical model, which was employed to simulate the device in ideal ocean conditions. The model was designed for the intention of improving the original NSPA WEC concept. The model was further improved through the implementation of optimization methods designed to determine optimum design specifications depending on the wave field.

Wave energy converters of all types remain under development, testing, and refinement. The NSPA WEC design incorporates the use of a buoy linked to a PTO mechanism through the use of a magnetic coupling system described in WIPO (PCT) application PCT/US13/42597 (to be published on December 2013). The direct movement from the buoy then causes the rotational motion of the ball screw to turn an alternator and produce power output. The first-generation prototype NSPA WEC constructed at the University of Massachusetts Dartmouth was capable of producing instantaneous power on the order of 100 W in the laboratory by lifting and dropping the buoy. Although this testing procedure does not necessarily mimic true wave motion, it provides a simple qualitative assessment of performance under conditions that may be significantly less in magnitude than coastal wave forces.

In addition to the development of the NSPA WEC, a numerical model was designed and successfully created in Python for the intention of simulating the NSPA WEC dynamics in an ideal ocean environment. Simulations were performed to show how the optimization routine can drastically improve performance for a given wave field. The results of the model simulations determined the model sensitivity to the radius of the buoy and ball screw lead variables. An optimization routine was employed to determine the optimal configuration of the buoy radius and ball screw for a variety of wave amplitudes for a given wave period of T = 1 s. The optimization simulations performed on the buoy radius and screw lead revealed the optimal range of values, which were used to determine the specific case used for the optimized single test run shown in Figure 4. The results of the optimized output of the simulation showed the buoy capable of tracking the motion of the wave field with higher accuracy, and the power output had increased such that the system operated at 9% efficiency. The radius of the buoy was calculated from the optimization routine using the alternator parameters provided by the WindBLU three-Phase AC PMA alternator. The NSPA WEC first-generation prototype was built with off-the-shelf parts, and our initial model analysis used these input values. It follows that the exceptionally large buoy radius can be attributed to the use of wind turbine alternator specifications, which require large blade lengths and high torques for operation.

The examples of numerical model output presented and discussed here are intended to illustrate the effectiveness of the modeling technique in guiding design decisions and in building intuition about system performance. As a realistic design tool, the model will be used to explore a much wider range of configurations than reported here, evaluating a number of different alternator options as well as variability in other mechanical, electrical, and environmental parameters. Moving forward, the model will be used in this mode to identify an ideal suite of design parameters for providing acceptable power output and efficiency for parameters within specified ranges, depending on the target implementation location. For instance, the ideal nearshore device may have buoy radii on the order of 0.5–1.0 m and a relatively small wave environment, while a device designed for offshore use may have a much larger radius and more energetic waves. It should also be noted that the model presented here has been designed explicitly to model the mechanical components of the system. Certain elements of wave modeling, such as wave diffraction and its feedback to the system, have not been addressed at this level of design modeling, which is intended as a first-order modeling exercise to provide insight into the appropriate ranges for design variables under given conditions. Intensive physical testing of prototypes designed using the modeling technique described here will be evaluated against model results and will provide feedback to determine higher levels of sophistication in the modeling procedure as warranted.

Acknowledgments

This project was made possible from funding through DOE Award Number DE-EE0000299, the University of Massachusetts Physics Department, the Intercampus Marine Science Program, and MREC. We would also like to thank the senior design wave energy team, Craig Nathan, Amy Lopes, and Justin Cantara for their strong

work and effort in this project. Finally, we would like to thank the faculty in the Physics Department and the faculty at SMAST for their guidance and support in performing this project. This manuscript is contribution XX-XXX in the SMAST Contribution Series, School for Marine Science and Technology, University of Massachusetts Dartmouth.

Authors:

Brandon E. Green and
Daniel G. MacDonald
University of Massachusetts
Dartmouth
School for Marine Science
and Technology
Department of Estuarine and
Ocean Sciences
200 Mill Road, Suite 325
Fairhaven, MA 02719
Email: bgreen1@umassd.edu;
dmacdonald@umassd.edu

References

Agamloh, E.B., Wallace, A.K., & von Jouanne, A. 2007. A novel direct-drive ocean wave energy extraction concept with contactless force transmission system. Renew Energ. 33(3):520-9. http://dx.doi.org/10.1016/j.renene.2007.01.008.

Agamloh, E.B., Wallace, A.K., & von Jouanne, A. 2008. Application of fluid-structure interaction simulation of an ocean wave energy extraction device. Renew Energ. 33:748-57. http://dx.doi.org/10.1016/j.renene.2007.04.010.

Bostrom, C. 2011. Electrical systems for wave energy conversion. Ph.D. Thesis, Uppsala University.

Callaghan, J., & Boud, R. 2006. Future Marine Energy. London: The Carbon Trust. 7 pp.

Clement, A., McCullen, P., Falcao, A., Fiorentino, A., Gardner, F., Hammarlund, K., … Thorpe, T. 2002. Wave energy in Europe: Current status and perspectives. Renew Sust Energ Rev. 6:405-31. http://dx.doi.org/10.1016/S1364-0321(02)00009-6.

Cruz, J. 2008. Ocean Wave Energy. Berlin, Germany: Springer-Verlag. pp. 93-104. http://dx.doi.org/10.1007/978-3-540-74895-3.

Danielsson, O. 2006. Wave energy conversion. Ph.D. Thesis, Uppsala University.

Drew, B., Plummer, A.R., & Sahinkaya, M.N. 2009. A review of wave energy converter technology. P I Mech Eng A-J Pow. 223:887-902. http://dx.doi.org/10.1243/09576509JPE782.

Engstrom, J. 2011. Hydrodynamic modeling for a point absorbing wave energy converter. Ph.D. Thesis, Uppsala University. pp. 55-7.

Eriksson, M. 2007. Modeling and experimental verification of direct drive wave energy conversion. Ph.D. Thesis, Uppsala University. 40 pp.

Eriksson, M., Isberg, J., & Leijon, M. 2005. Hydrodynamic modeling of a direct drive wave energy converter. Int J Eng Sci. 43:1377-87. http://dx.doi.org/10.1016/j.ijengsci.2005.05.014.

Falnes, J. 2007. A review of wave-energy extraction. Mar Struct. 20:185-201. http://dx.doi.org/10.1016/j.marstruc.2007.09.001.

Griffiths, D. 1999. Introduction to Electrodynamics. Upper Saddle River, NJ: Prentice Hall. 326 pp.

Henderson, R. 2006. Design, simulation, and testing of a novel hydraulic power take-off system for the Pelamis wave energy converter. Renew Energ. 31:271-83. http://dx.doi.org/10.1016/j.renene.2005.08.021.

Ivanova, I.A., Bernhoff, H., Agren, O., & Leijon, M. 2005. Simulated generator for wave energy extraction in deep water. Ocean Eng. 32:1664-78. http://dx.doi.org/10.1016/j.oceaneng.2005.02.006.

Kofoed, J., Frigaard, P., & Friid-Madsen, E. 2006. Sorensen H. prototype testing of the wave energy converter wave dragon. Renew Energ. 31:181-9. http://dx.doi.org/10.1016/j.renene.2005.09.005.

Kundu, P., & Cohen, I. 2008. Fluid Mechanics. Burlington, MA: Academic Press. 273 pp.

Leijon, M., Bernhoff, H., Agren, O., Isberg, J., Sundberg, J., Berg, M., & Karlsson, K.E. 2010. Multiphysics simulation of wave energy to electric energy conversion by permanent magnet linear generator. In: IEEE Transactions on Energy Conversion. 1-6, 2004. M. McCormick. Ocean Engineering Mechanics. New York: Cambridge University Press.

Leijon, M., Danielsson, O., Eriksson, M., Thorburn, K., Bernhoff, H., Isberg, J., … Wolfbrandt, A. 2006. An electrical approach to wave energy conversion. Renew Energ. 31:1309-19. http://dx.doi.org/10.1016/j.renene.2005.07.009.

McCormick, M. 2010. Ocean Engineering Mechanics. New York: Cambridge University Press. 64 pp.

Mueller, M.A. 2002. Electrical generators for direct drive wave energy converters. IEE Proc-C. 149:446-56.

Ocean Power Technologies. 2010. OPT Technologies Annual Report 2010. 10 Apr 2010. http://www.oceanpowertechnologies.com.

Pelc, R., & Fujita, R. 2002. Renewable energy from the ocean. Mar Policy. 26:471-9. http://dx.doi.org/10.1016/S0308-597X(02)00045-3.

Polinder, H., Damen, M., & Gardner, F. 2004. Linear PM generator system for wave energy conversion in the AWS. IEEE T Energy Conver. 19:583-9. http://dx.doi.org/10.1109/TEC.2004.827717.

Press, W. 2007. Numerical Recipes: The Art of Scientific Computing 3rd Edition. Cambridge, New York: Cambridge University Press. 907 pp.

Rhinefrank, K., Agamloh, E.B., Jouanne, A., Wallace, A.K., Prudell, J., Kimble, K., … Schacher, A. 2006. Novel ocean energy permanent magnet linear generator buoy. Renew Energ. 31:1279-98. http://dx.doi.org/10.1016/j.renene.2005.07.005.

Salter, S.H. 1974. Wave power. Nature. 249:720-4. http://dx.doi.org/10.1038/249720a0.

Simoes, M., & Farret, F. 2004. Renewable Energy Systems: Design and Analysis with Induction Generators. New York: CRC Press LLC. 358 pp.

Sorensen, B. 2004. Renewable Energy. New York: Elsevier Science. pp. 24-5.

Thorburn, K. 2006. Electric energy conversion systems: Wave energy and hydropower. Ph.D. Thesis, Uppsala University.

Thorpe, T.W. 1998. An Overview of Wave Energy Technologies, AEAT-3615 for the Marine Foresight Panel.

Thorpe, T.W. 1999. A Brief Review of Wave Energy. ETSU Report R-120 for the UK Department of Trade and Industry.

Tyrberg, S. 2009. Studying buoy motion for wave power. Ph.D. Thesis, Uppsala University.

Vining, J. 2005. Ocean wave energy conversion. Master's Thesis, University of Wisconsin.

Watanabe, T., & Suzuki, K. 2004. Experimental study on ball screw type magnetic friction damper: Semiactive control using electromagnet. ASME. 126:110-4.

Waters, R. 2008. Energy from ocean waves. Ph.D. Thesis. Uppsala University.

Waters, R., Rahm, M., Eriksson, M., Svensson, O., Strömstedt, E., Boström, C., … Leijon, M. 2011. Ocean wave energy absorption in response to wave period and amplitude—Offshore experiments on a wave energy converter. IET Renew Power Gen. 5:465-9. http://dx.doi.org/10.1049/iet-rpg.2010.0124.